Near-infrared Persistent Luminescence and Trap Re-shuffling in Mn^{4+} Doped Alkali-earth Metal Tungstates

Jiaren Du, Kai Li, Rik Van Deun, Dirk Poelman*, Hengwei Lin*

Dr. Jiaren Du, Prof. Hengwei Lin
International Joint Research Center for Photo-responsive Molecules and Materials, School of Chemical and Material Engineering, Jiangnan University, 214122, Wuxi, China.
E-mail: *Dr. Jiaren Du* (jiaren.du@jiangnan.edu.cn)

Prof. Dirk Poelman
LumiLab, Department of Solid State Sciences, Ghent University, Krijgslaan 281-S1, B-9000, Ghent, Belgium.
Center for Nano- and Biophotonics (NB-Photonics), Ghent University, B-9000, Ghent, Belgium.
E-mail: *Prof. Dirk Poelman* (dirk.poelman@ugent.be)

Dr. Kai Li, Prof. Rik Van Deun
L^3–Luminescent Lanthanide Lab, Department of Chemistry, Ghent University, Krijgslaan 281-S3, B-9000 Ghent, Belgium.

Keywords: NIR emission, persistent luminescence, thermoluminescence, photo-stimulated de-trapping, $Sr_2Ca_{0.9}La_{0.1}W_{0.995}O_6$:0.005$Mn^{4+}$

Near-infrared persistent luminescent materials have great potential for *in vivo* bioimaging and night-vision surveillance due to their long-lasting autofluorescence-free emission through deep tissues and multi-cycle photo-stimulated luminescence by releasing energy from captured traps using high-intensity 808 nm or 980 nm lasers. However, phosphors combining both near-infrared persistent luminescence and photo-stimulated luminescence are found mostly in chromium doped gallates hosts, other emitters are rarely reported. Herein, a new material system with near-infrared persistent luminescence is achieved in tetravalent manganese doped double-perovskite alkali-earth metal tungstates via the aliovalent substitution of calcium ions with lanthanum ions. Persistent luminescence could be generated via X-ray irradiation, providing great promise in long-term deep-tissue ultrasensitive imaging, information storage

and X-ray detection. Photo-stimulated de-trapping is successfully demonstrated using a common 420 nm light emitting diode instead of a high-intensity 808 nm or 980 nm laser. The traps distribution is proved to be re-shuffled upon this laser-free visible light stimulation. Re-shuffling of trap distributions upon visible light stimulation may be promising for optical information storage applications. This work is expected to broaden the range of near-infrared persistent material systems and provides new insights into manipulating photo-stimulated traps via laser-free light stimulation.

1. Introduction

Persistent luminescence, also known as long-lasting afterglow, is a particular optical phenomenon where light emission continues for seconds, minutes or hours after the excitation source ceases. Thermally assisted de-trapping with the probability depending on ambient temperature and trap depth, is the key process dominating persistent luminescence in glow-in-the-dark phosphors or persistent phosphors. To date, persistent phosphors have been widely applied in the fields of luminous paints, safety displays, emergency signage, information storage, alternating current-driven light emitting diodes and artificial synapses[1, 2, 3, 4, 5]. The utilization of near-infrared (NIR) persistent luminescence for in vivo imaging brought NIR persistent phosphors into the bio-imaging field. By using a high-intensity 808 nm or 980 nm laser, repeated long-term imaging can obtained from photo-stimulated luminescence via releasing energy from captured traps[6, 7]. A large number of phosphors showing long-lasting persistent luminescence in the NIR region have been synthesized, and ultraviolet (UV) light has been widely applied to excite persistent luminescence[8]. Recently, red or deep-red light (600-800 nm) has also been investigated to serve as excitation source for multi-cycle long-term bioimaging[9, 10, 11, 12]. However, there is still a limitation for deep penetration and high signal-

to-noise ratio imaging due to the lack of phosphors allowing NIR in vivo excitation. Persistent luminescence excited in situ by X-rays was reported in chromium-doped gallates[13, 14, 15]. Compared to light, X-rays have deep penetration of tissues and show great promise in long-term deep-tissue ultrasensitive imaging[13, 16].

Cr^{3+} and Mn^{4+} transition metal ions, with $3d^3$ electron configurations, are ideal NIR emitters[17, 18]. Cr^{3+} or Mn^{4+} ions are usually stabilized and situated in octahedral symmetry environment of many host matrices[19]. In regard to NIR persistent luminescence, great progress has been made in the development of Cr^{3+} doped NIR persistent phosphors and there is a long list of candidate NIR emitters [20, 21, 22]. For instance, the gallate system with octahedral coordination environments is regarded as the preferred host for preparing Cr^{3+} doped NIR persistent phosphors[23, 24]. Some representative examples are $ZnGa_2O_4:Cr^{3+}$[25], $MgGa_2O_4:Cr^{3+}$[26], $LiGa_5O_8:Cr^{3+}$[27], $Zn_{1+x}Ga_{2-2x}(Ge/Sn)_xO_4:Cr^{3+}$[28], $Mg_{1+x}Ga_{2-2x}Ge_xO_4:Cr^{3+}$[29], and $Y_3Al_2Ga_3O_{12}:Cr^{3+}$[30]. In contrast, the numbers of the Mn^{4+} doped candidates with NIR persistent luminescence are very limited[31]. To the best of our knowledge, only aluminates and germanates have been explored[32, 33]. The search for new candidates is prerequisite and the development of Mn^{4+} doped NIR persistent materials is still an ongoing challenge.

Tungstates with facile synthesis, low cost and good chemical stability are suitable host materials for rare earth metal and transition metal doping. Recently, a facile strategy was reported for co-doping Ln^{3+} (Ln = La, Gd, Y, Lu) and Mn^{4+} in the double-perovskite Sr_2CaWO_6 compound[34]. Efficient steady-state luminescence and extraordinary thermal stability were achieved. In this work, near-infrared persistent luminescence was reported in tetravalent manganese doped double-perovskite alkali-earth metal tungstates via the aliovalent substitution of calcium ions (Ca^{2+}) with lanthanum ions (La^{3+}). A detailed spectral characterization and a series of thermoluminescence (TL) measurements were made to shed light on trapping and de-trapping

processes of this Mn^{4+} doped new material system with long-lasting NIR emission. From an application point of view, it is important to get a grasp of the manipulation of photo-stimulated traps in a laser-free way. Manipulation of traps in an optical write-in and read-out approach is necessary for optical information storage, but the effect is often underestimated. By employing a 420 nm light emitting diode, photo-stimulated de-trapping was successfully demonstrated. Moreover, the trap distribution was proved to be re-shuffled upon this laser-free light stimulation. More importantly, re-shuffling trap distributions upon visible light stimulation may be promising for optical information storage applications. In addition, persistent luminescence could be generated via X-ray irradiation, showing great promise in long-term deep-tissue ultrasensitive imaging, information storage and X-ray detection. This work offers an example of the exploration of novel NIR persistent phosphors and provides new insights into manipulating photo-stimulated traps in a laser-free way.

2. Results and Discussion

2.1. Photoluminescence, persistent luminescence and thermoluminescence

The chemical composition of $Sr_2Ca_{0.9}La_{0.1}W_{0.995}O_6$:0.005$Mn^{4+}$ was investigated as a representative example. Photoluminescence excitation and emission spectra as well as the persistent luminescence excitation spectrum of $Sr_2Ca_{0.9}La_{0.1}W_{0.995}O_6$:0.005$Mn^{4+}$ phosphors are shown in Figure 1. Upon 336 nm excitation, the emission spectrum presents narrow-band profiles centered at 677 nm typical for Mn^{4+}[18, 35] (**Figure 1**a). However, the individual components of the zero phonon R line with their Stokes and anti-Stokes phonon side bands cannot be resolved in $Sr_2Ca_{0.9}La_{0.1}W_{0.995}O_6$:0.005$Mn^{4+}$ phosphors mainly due to instrument resolution and insufficiently low temperature. The emission is attributed to the parity and spin-forbidden $^2E_g \rightarrow {}^4A_{2g}$ transition of Mn^{4+} ions located in WO_6 octahedra. The broad excitation spectrum (λ_{em} = 677 nm) ranging from 250 to 550 nm with a maximum at 336 nm originates

from the contribution of Mn^{4+}–O^{2-} charge transfer, spin-allowed $^4A_{2g} \rightarrow {}^4T_{1g}$, spin-forbidden $^4A_{2g} \rightarrow {}^2T_{2g}$ and spin-allowed $^4A_{2g} \rightarrow {}^4T_{2g}$ transitions of Mn^{4+}, consistent with the Tanabe-Sugano diagram for a d3-configuration in an octahedral environment[36, 37, 38]. The main peak at 336 nm can be assigned to the overlap between the Mn^{4+}–O^{2-} charge transfer band and the spin-allowed $^4A_{2g} \rightarrow {}^4T_{1g}$ transition of Mn^{4+} ions. The persistent luminescence excitation spectrum of $Sr_2Ca_{0.9}La_{0.1}W_{0.995}O_6$:0.005$Mn^{4+}$ (in Figure 1b) presents the wavelength range for charging NIR persistent luminescence. Decay profiles were monitored at 677 nm after 3-min excitation with monochromatic light ranging from 240 to 600 nm. The persistent luminescence intensity was plotted as a function of the excitation wavelength by integrating the decay profiles during the first 2 minutes of afterglow (see details in Figure S1). Although the steady state photoluminescence of the $Sr_2Ca_{0.9}La_{0.1}W_{0.995}O_6$:0.005$Mn^{4+}$ phosphor can be excited upon UV and visible excitation spectral range (from 250 to 550 nm, as seen in Figure 1a), NIR persistent luminescence can only be effectively obtained in a narrow range of excitation wavelengths (ranging from 250 to 330 nm). The cutoff wavelength (λ_{cutoff}) for activating persistent luminescence is estimated around 340 nm, which is the lowest cutoff value among Mn^{4+} doped persistent phosphors[9]. It is worth mentioning that a commonly used 365-nm 'black light' UV light source cannot induce persistent luminescence in the $Sr_2Ca_{0.9}La_{0.1}W_{0.995}O_6$:0.005$Mn^{4+}$ phosphor, in spite of the bright steady-state NIR emission under 365 nm irradiation (as shown in Figure S2). This excitation wavelength dependent persistent luminescence is also proved by the thermoluminescence measurements upon different charging sources (254, 365 and 420 nm) in Figure S3. Upon 365 nm or 420 nm charging, there were no TL peaks and traps were not filled. In contrast, it can be seen that 254 nm UV charging can effectively fill traps with the presence of a broad TL peak spanning from room temperature to 100 °C.

The persistent luminescence decay profiles of $Sr_2Ca_{0.9}La_{0.1}W_{0.995}O_6$:0.005$Mn^{4+}$ phosphor after 3-min xenon arc lamp excitation were recorded at room temperature, as shown in **Figure 2**. The logarithmic plot of the afterglow intensity was given as a function of time in the main figure, and the reciprocal plot of intensity was also inserted in Figure 2. Measuring afterglow intensity in radiometric units instead of arbitrary units, makes it possible to compare the afterglow decay performance among other persistent phosphors. Usually, 0.32 mcd/m^2 is defined as threshold for the visible afterglow emission, and this value is replaced by the equivalent radiometric unit of mW/sr/m^2 for NIR emission[39]. Hereby, 10^{-3} mW/sr/m^2 is roughly equivalent to 0.32 mcd/m^2. The afterglow duration of $Sr_2Ca_{0.9}La_{0.1}W_{0.995}O_6$:0.005$Mn^{4+}$ is estimated at around 20 minutes when the intensity drops below the threshold value of 10^{-3} mW/sr/m^2. Such afterglow duration is the longest among all reported Mn^{4+} doped persistent phosphors in literature, such as La_2MgGeO_6:Mn^{4+}[32], $LaAlO_3$:Mn^{4+}[40] and $La_{1-x}Gd_xAlO_3$:Mn^{4+}[41]. Persistent luminescence, steady-state photoluminescence and thermoluminescence spectrum of $Sr_2Ca_{0.9}La_{0.1}W_{0.995}O_6$:0.005$Mn^{4+}$ phosphor were recorded using the same detector and compared in **Figure 3**. After ceasing the UV excitation source, the afterglow spectra were collected at 10 s, 30 s, 60 s, 150 s and 200 s, respectively (in Figure 3a). The photoluminescence spectrum was obtained upon 365-nm UV source excitation (in Figure 3b), and the thermoluminescence spectrum was recorded at 25 °C during the linear heating stage (Figure 3c). TL glow curves represent the plot of integrated emission intensity as a function of the temperature (the linear temperature rises with a constant heating rate). However, a TL spectrum provides the plot of emission intensity as a function of wavelength at a certain temperature. It is clear that all the positions of emission peaks are located around 677 nm. Chromatic coordinates for persistent luminescence, photoluminescence and thermoluminescence were given in Figure S4. All CIE coordinates were sited in deep-red region, suggesting their potential for LEDs in agricultural applications. The almost same CIE coordinates and similar features among three kinds of spectra indicate that the NIR emissions (photoluminescence, persistent

luminescence, and thermoluminescence) originate from the same Mn^{4+}-emitting centers in each luminescence process.

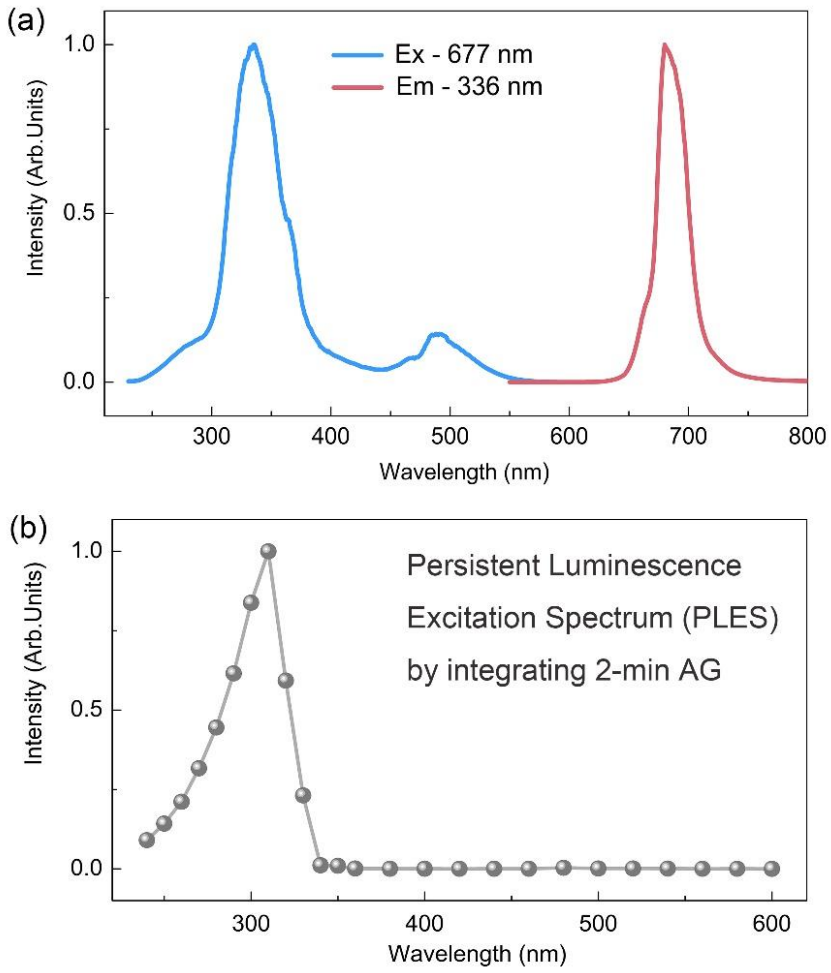

Figure 1. (a) Photoluminescence (PL) and photoluminescence excitation (PLE) spectra of $Sr_2Ca_{0.9}La_{0.1}W_{0.995}O_6$:0.005$Mn^{4+}$ phosphor. The blue line is the excitation spectrum probed at an emission wavelength of 677 nm, and the red line is the emission spectrum obtained with excitation at 336 nm. (b) Persistent luminescence excitation spectrum of $Sr_2Ca_{0.9}La_{0.1}W_{0.995}O_6$:0.005$Mn^{4+}$ phosphor.

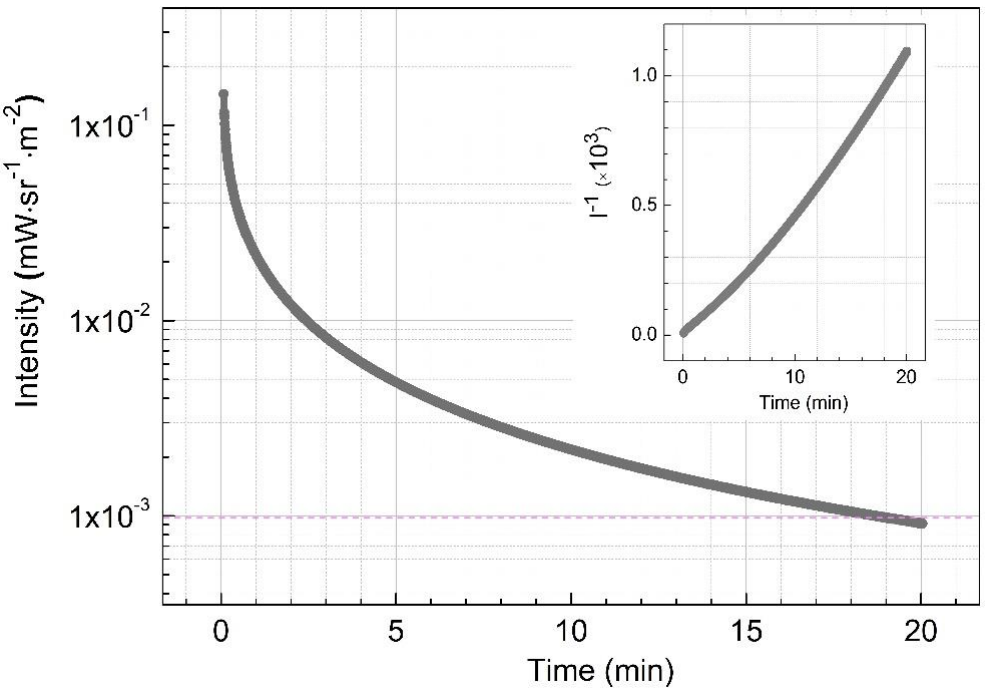

Figure 2. Persistent luminescence decay of $Sr_2Ca_{0.9}La_{0.1}W_{0.995}O_6$:0.005$Mn^{4+}$ as a function of time. The inset shows the inverse intensity as a function of time.

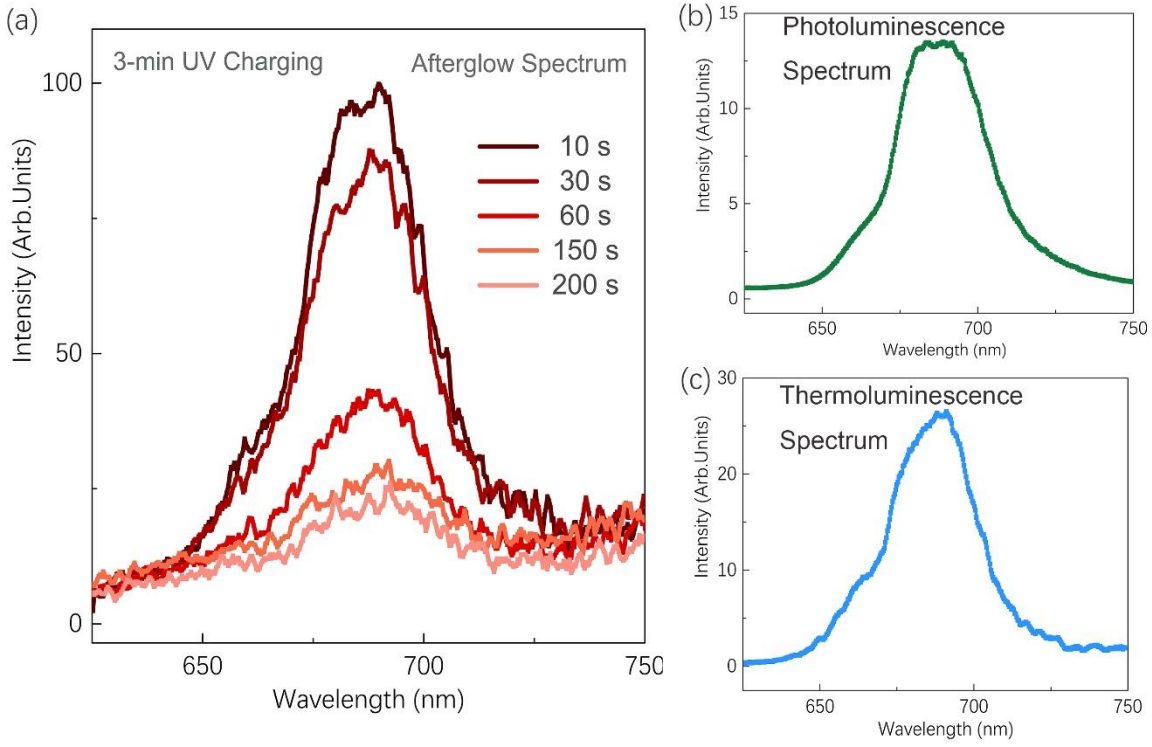

Figure 3. Persistent luminescence (a), photoluminescence (b) and thermoluminescence spectrum (c) of $Sr_2Ca_{0.9}La_{0.1}W_{0.995}O_6$:0.005$Mn^{4+}$ phosphor.

2.2. Trapping and de-trapping.

The influence of charging temperature during 254 nm UV excitation on the trapping efficiency of $Sr_2Ca_{0.9}La_{0.1}W_{0.995}O_6$:0.005$Mn^{4+}$ phosphor was evaluated using thermoluminescence measurements, as shown in **Figure 4**a. Two main TL glow peaks (Peak I centered around -25 °C and Peak II around 50 °C) were present when charging was performed at very low temperature (-60 °C). Increasing the charging temperature from -60 °C to 0 °C, led to the increase of TL intensity, but the shallow trap (Peak I) started to be emptied due to the elevated ambient energy. A shift of the TL glow peak towards higher temperature was observed with further increasing charging temperature, indicating only the deeper traps remained filled at elevated ambient condition. These observations are consistent with what can be expected for phosphors with multiple trap depths and broad trap distributions[*42, 43*]. Figure 4b presents the total trapping storage capacity as a function of charging temperature by integrating TL glow curves of Figure 4a. The charging temperature of 20 °C displayed yielded the most trapping storage. In addition, by employing a longer charging duration, trapping storage was improved and the position of TL peaks moved to higher temperature (deeper traps were filled, as shown in Figure 4c).

The temperature dependent afterglow output (de-trapping process) was studied using a series of fading experiments (with a fading time of 15 min or without fading between irradiation and heating stage) at variable ambient temperatures in **Figure 5**. TL glow curves of $Sr_2Ca_{0.9}La_{0.1}W_{0.995}O_6$:0.005$Mn^{4+}$ at variable charging and fading temperatures (starting from -25 °C to 37 °C) are given in Figure 5a, b and Figure S5. Obviously, a 15-min fading between irradiation and heating stage leads to the thermal release of charge carriers (de-trapping at

fading ambient temperatures). The low-temperature side (the lower trap energy levels) was initially emptied and the position of TL peaks moved to higher temperature with elevated fading conditions. The trapping storage capacity (the number of charge carriers trapped), with and without fading, can be obtained from Figure 5a and b. It has been reported that $Sr_2Ca_{0.9}La_{0.1}W_{0.995}O_6$:0.005$Mn^{4+}$ shows a good thermal stability and has a limited luminescence thermal quenching (94.8% of the RT intensity remaining at 478 K)[34]. Thus, the area under TL glow curve without fading can be regarded as a measure for the total number of charge carriers filled during charging, while the area below the TL glow curve after 15-min fading is proportional to the number of charge carriers remained. Figure 5c plots two curves for the number of charge carriers trapped before and after 15-min fading, as a function of fading temperature. The difference between the two curves (Figure 5c) provides the fading temperature dependent afterglow output in Figure 5d. The afterglow output at 25 °C or 37 °C is quite high, indicating that most of trapped charge carriers are de-trapping with light emission, which is in line with the temperature dependent afterglow decay curve in Figure 5e. Although there is a strong initial afterglow intensity at 37 °C (AG 37 °C, red line), the afteglow intensity drops and the decay curve falls below that at 25 ° (AG 25 °C, green line) in Figure 5e. These afterglow decay observations are consistent with the fact that the amount of de-trapped charge carriers at 37 °C is fewer than that at 25 °C during the 15 min fading (Figure 5d). From an application point of view, it is important to get a grasp of the trapping and de-trapping behavior. When persistent phosphors are applied in outdoor conditions, it is essential to know their afterglow performance at variable working environments. Considering the discussion above, however, $Sr_2Ca_{0.9}La_{0.1}W_{0.995}O_6$:0.005$Mn^{4+}$ is not favorable for low-temperature (< 0 °C) working conditions due to the low trap filling efficiency and limited afterglow output.

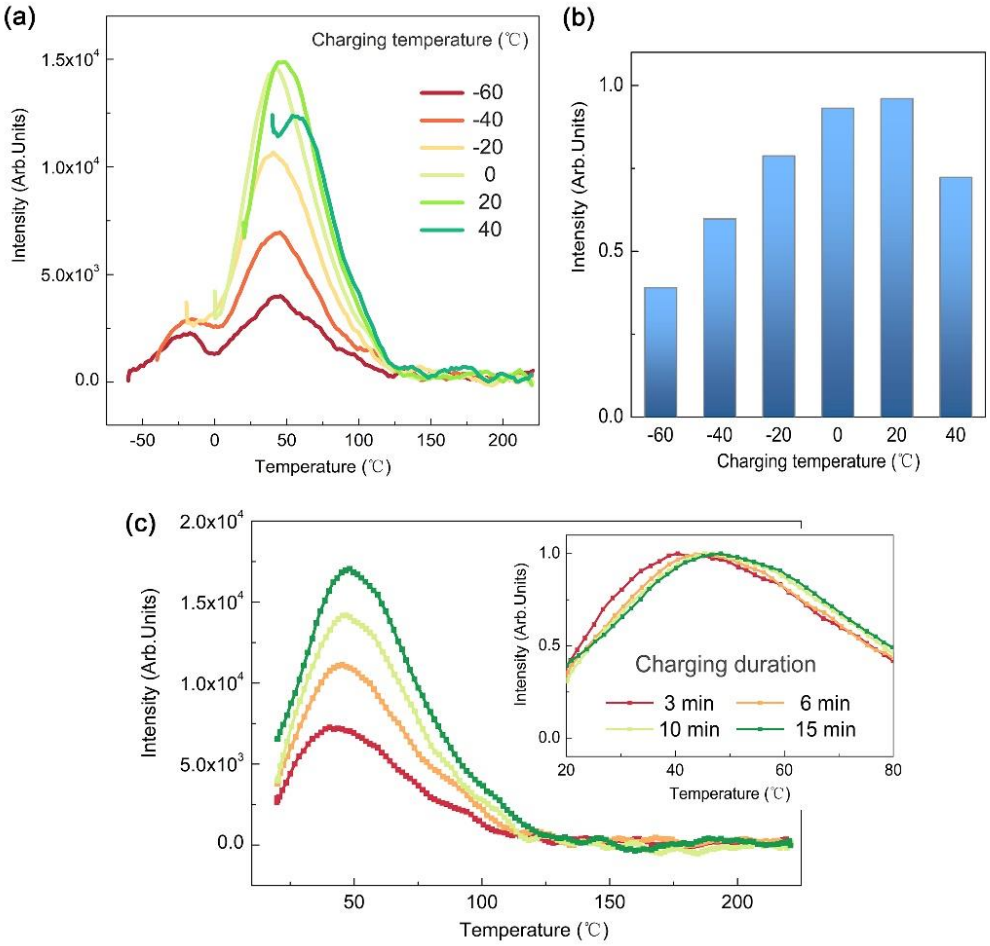

Figure 4. Charging temperature and charging duration dependent thermoluminescence. (a) TL glow curves at different charging temperatures from -60 °C to 40 °C; (b) Total trapping storage capacity as a function of charging temperature; (c) TL glow curves upon different charging durations, and the normalized TL glow curves in the insert.

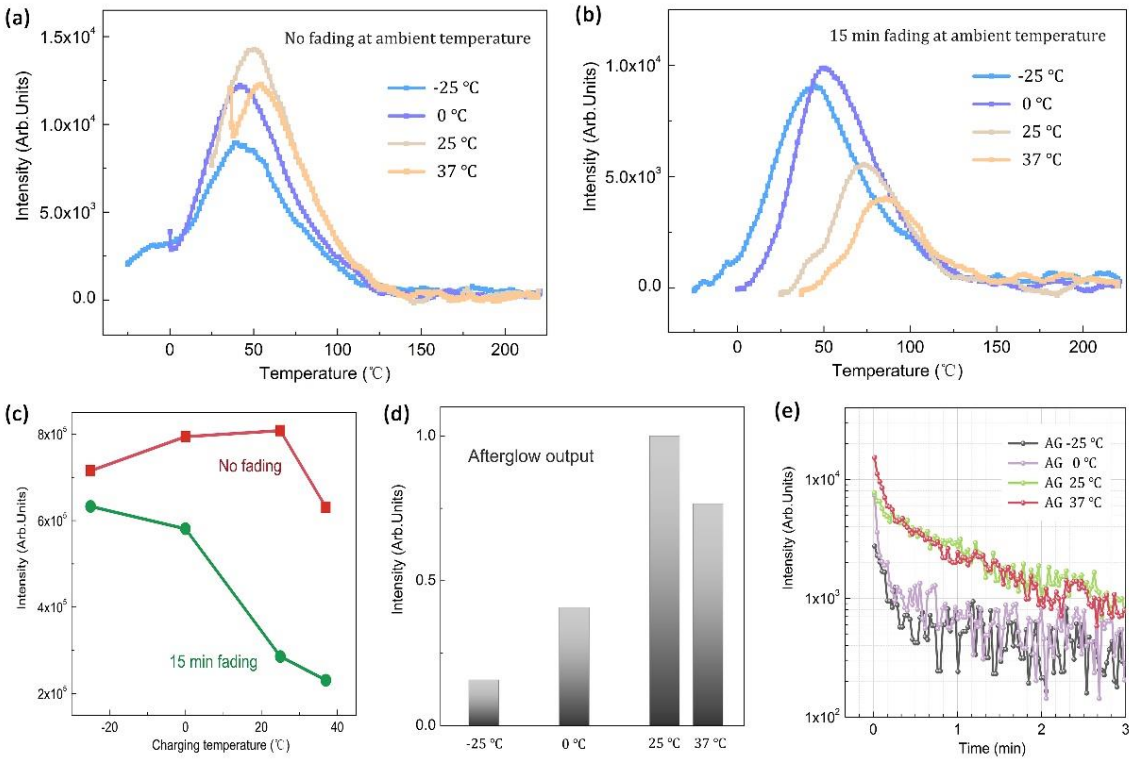

Figure 5. Fading temperature dependent de-trapping process of $Sr_2Ca_{0.9}La_{0.1}W_{0.995}O_6$:0.005$Mn^{4+}$. TL glow curves with (a) no fading, or (b) fading for 15 minutes at ambient temperature; (c) charge carriers trapped before and after 15-min fading as a function of fading temperature; (d) fading temperature dependent afterglow output; (e) afterglow decay curves at different ambient temperatures (-25, 0, 25, and 37 °C).

De-trapping is usually believed to be a thermally activated process with the aid of ambient thermal energy[42, 43, 44]. Figure S6 provides TL glow curves of $Sr_2Ca_{0.9}La_{0.1}W_{0.995}O_6$:0.005$Mn^{4+}$ after different low-temperature fading durations (0, 5, 10, and 15 min) at -50 °C. There was little difference between the TL glow curves and energy was barely released due to the insufficient thermal energy at low temperature of -50 °C. In $Sr_2Ca_{0.9}La_{0.1}W_{0.995}O_6$:0.005$Mn^{4+}$, both thermally activated de-trapping and optically stimulated de-trapping can be achieved, as identified in **Figure 6**. Optically stimulated de-trapping is performed using a second light source

with a longer wavelength (for instance, a common 420 nm LED) rather than the 254 nm charging source. Typical thermally activated de-trapping can be found from TL glow curves after 5-min fading. On the other hand, the contribution from optically stimulated de-trapping can also be clearly seen when the 420 nm LED was on during the 5-min fading. In Figure 6a, the drop of TL intensity for 5-min fading (LED On) indicates the coexistence of thermally and optically activated de-trapping in $Sr_2Ca_{0.9}La_{0.1}W_{0.995}O_6$:0.005$Mn^{4+}$. Increasing the illumination intensity by increasing the current of the 420 nm LED, the amount of released charge carriers increased accordingly (thus the TL intensity decreased in Figure 6b).

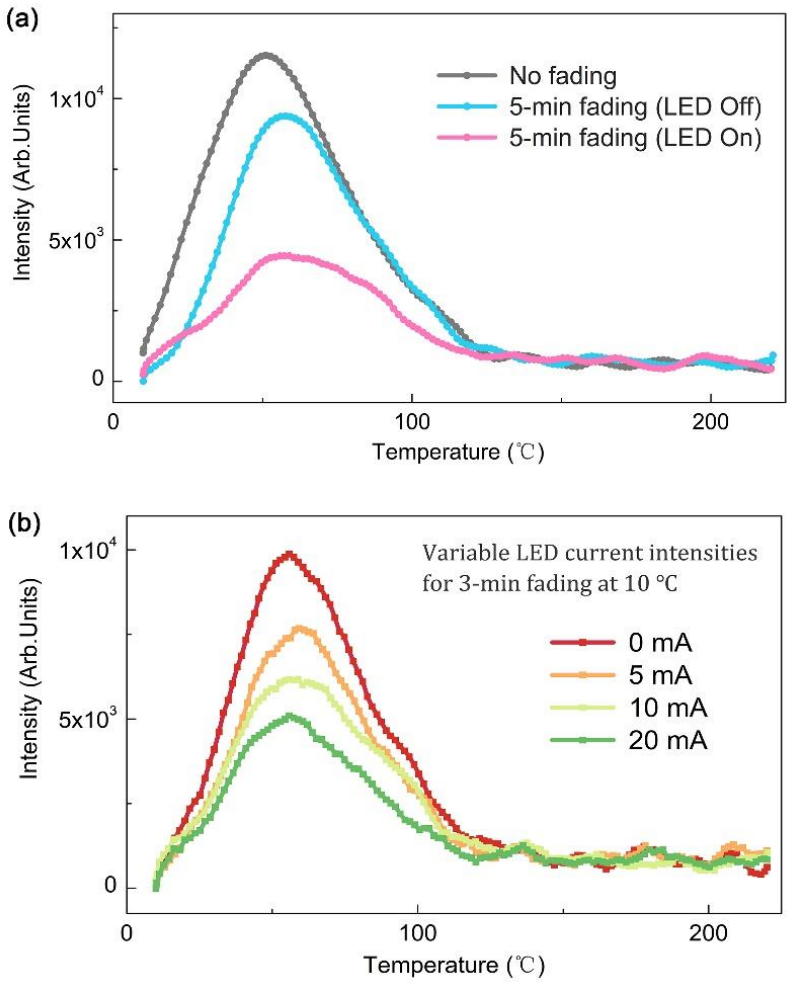

Figure 6. De-trapping process of $Sr_2Ca_{0.9}La_{0.1}W_{0.995}O_6$:0.005$Mn^{4+}$ upon 420 nm illumination. (a) TL glow curves were recorded without fading or with 5-min fading (LED Off). Illumination from 420 nm LED was also shed on sample (LED On) during

the 5-min fading; (b) TL glow curves after variable illumination intensities from 420 nm LED.

2.3. Re-shuffling traps distribution.

Charge transfer processes among traps have been observed in several defect-involving luminescent materials[45, 46, 47]. To evaluate the possibility of charge transfer processes among traps, a low-temperature thermoluminescence experiment was designed (**Figure 7**). Trap filling of the $Sr_2Ca_{0.9}La_{0.1}W_{0.995}O_6$:0.005$Mn^{4+}$ was initially executed using 254 nm UV light at room temperature. Subsequently, the sample was quickly cooled down to -60 °C, at the same fading temperature to allow a comparison. Prior to recording the TL glow curve, a 420 nm LED illumination source was turned on (LED_{ON}) or off (LED_{OFF}), respectively, during the entire 3-min fading time at -60 °C. TL glow curves with LED_{ON} or LED_{OFF} were then measured, shown in Figure 7. In this way, the recorded TL glow curves can provide reliable information about which defect levels are influenced by light stimulation (420 nm LED_{ON}), together with comparison to the initial trap depth distribution from the TL glow curve in the absence of light stimulation (420 nm LED_{OFF}). The presence of the re-shuffling events is identified based on the changes of the TL glow curves (in Figure 7). Only one main TL peak centered around 50 °C ranging from room temperature to 120 °C was present if the 420 nm LED was off (as a reference), while multiple TL peaks appeared covering the range from -60 °C to 120 °C if the 420 nm LED was on. It is worth noting that the 420 nm LED illumination source cannot fill the traps as discussed above, thus the number of traps distributed from -60 °C to 0 °C (the red area) mainly comes from the charge transferred from the traps that are normally emptied from 20 °C to 120 °C (the green area). Such charge transfer process by a 420 nm LED is not common, and re-shuffling of a trap distribution has not been reported in Mn^{4+} doped persistent phosphors so far. Such re-shuffling event implies charge carriers are released under the influence of the

optical stimulation and occupy shallow-lying trap levels instead of leading purely to recombination at luminescent centers (the NIR emitter, Mn^{4+} ions in this case). In most re-shuffling events upon mechanical stimulation, the increase in the occupation of deep traps was observed[45, 46]. In contrast, the occupation of shallow-lying trap levels of $Sr_2Ca_{0.9}La_{0.1}W_{0.995}O_6$:0.005$Mn^{4+}$ was increased under 420 nm LED light stimulation. A partial emptying of the deep traps by photo-stimulation and re-trapping within defect energy levels contribute to the re-shuffling of trap occupations in the presence of light stimulation (such as light of 420 nm LED)

In addition, it is known that 254 nm UV light source usually works for the trap filling of persistent phosphors. Interestingly, 254 nm UV light is also able to reshuffle traps distributions in the case of $Sr_2Ca_{0.9}La_{0.1}W_{0.995}O_6$:0.005$Mn^{4+}$. A comparison of TL glow curves was made by tuning on or off 254 nm UV illumination during 3-min fading at -60 °C in **Figure 8** (here phosphor was initially charged at room temperature, and 254 nm UV light source act as both charging source and stimulation source). Moreover, a direct 254 nm UV charging at -60 °C was also displayed for comparison. Although the increase in the number of traps distributed from -60 °C to 0 °C should be partly attributed to the direct trap filling at -60 °C by UV light, it can be seen that 254 nm light source is also possible for traps distributions re-shuffling due to the decrease of the number of traps covering from 20 °C to 120 °C. That is to say, the excitation of 254 nm light played dual roles – trap filling and trap re-shuffling.

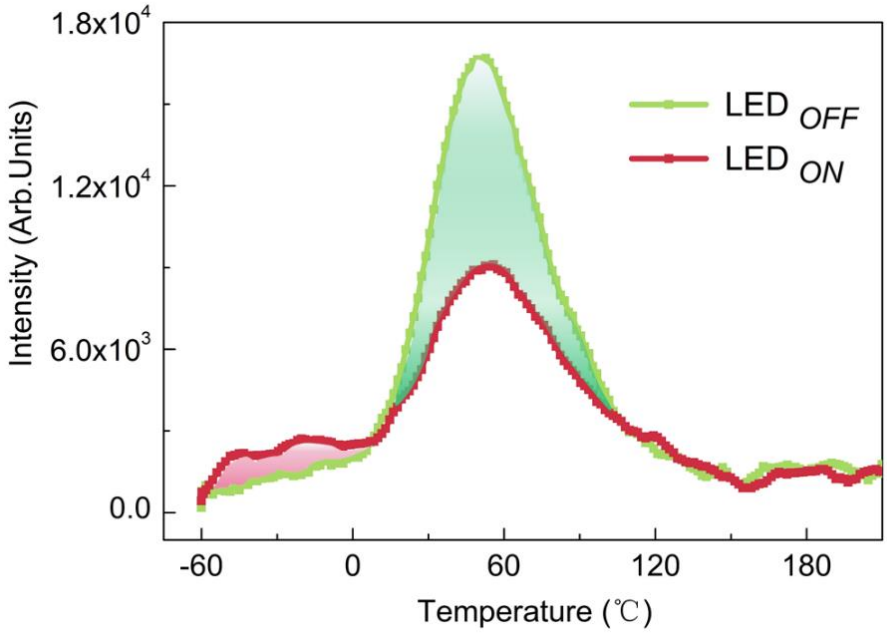

Figure 7. Re-shuffling trap distributions of $Sr_2Ca_{0.9}La_{0.1}W_{0.995}O_6$:0.005$Mn^{4+}$ upon 420 nm illumination.

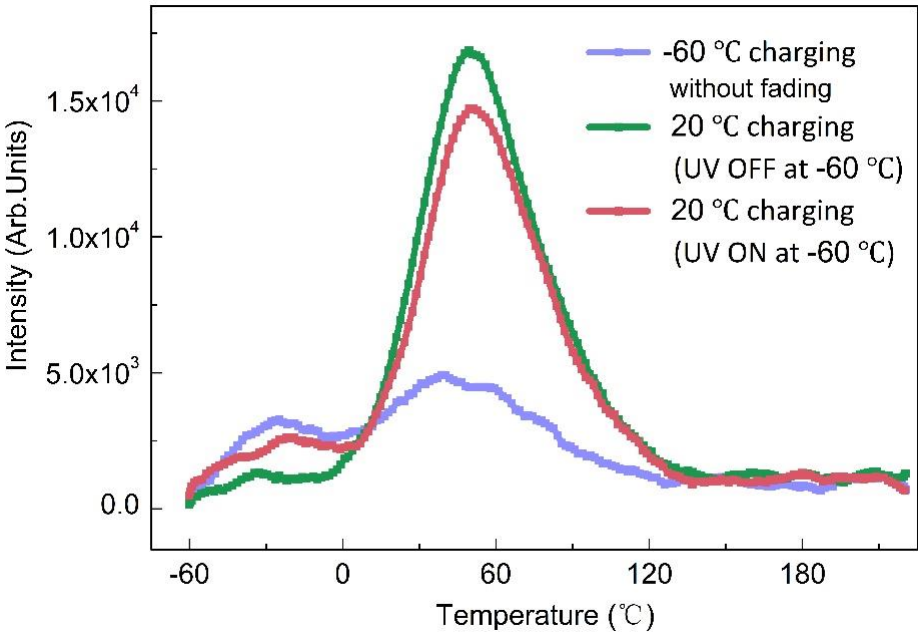

Figure 8. Re-shuffling trap distribution of $Sr_2Ca_{0.9}La_{0.1}W_{0.995}O_6$:0.005$Mn^{4+}$ upon 254 nm UV illumination

2.4. X-ray induced persistent luminescence and traps manipulation.

X-ray induced persistent luminescence and thermoluminescence from $Sr_2Ca_{0.9}La_{0.1}W_{0.995}O_6$:0.005$Mn^{4+}$ were investigated (**Figure 9**). In general, persistent phosphors require UV light to charge, which limits the energy enrichment and long-term signal tracking, especially in bioimaging purpose. By contrast, X-ray charging of persistent phosphors has been employed in deep tissue ultrasensitive imaging, and photodynamic therapy[13]. Apart from UV light (as discussed in the section on the persistent luminescence excitation spectrum), NIR persistent luminescence can also be induced using high-energy X-rays in $Sr_2Ca_{0.9}La_{0.1}W_{0.995}O_6$:0.005$Mn^{4+}$. Figure 9a presents a comparison of TL glow curves after UV and X-ray excitation. The shape of the TL glow curves and TL peak positions were similar, but a stronger TL intensity was found after X-ray charging, suggesting more traps were filled by X-rays presumably due to a stronger absorption cross section in the case of X-ray charging. NIR persistent luminescence was recorded as a function of time in Figure 9b. There is also a X-ray-dose effect, and more traps were filled with increasing X-ray irradiation durations (from 30 s to 300 s, as given in Figure 9c). These observations suggest a satisfactory light storage capacity in $Sr_2Ca_{0.9}La_{0.1}W_{0.995}O_6$:0.005$Mn^{4+}$ charged by X-rays, which may provide opportunities to biomedical technology and optical information storage. More impressively, trap distribution re-shuffling was also identified with charge transferred by using 420 nm LED stimulation. An initial 300 seconds X-ray irradiation was employed on $Sr_2Ca_{0.9}La_{0.1}W_{0.995}O_6$:0.005$Mn^{4+}$ at room temperature. In order to allow a comparison, the 420 nm LED illumination source was turned on or off, respectively, during the entire 1-min fading time at -60 °C (Figure 9d). Similar to previous observation upon UV irradiation in Figure 7, charge carriers induced by X-ray were released under the influence of the optical stimulation (420 nm LED) and the occupation of shallow-lying trap levels (covering from -60 °C to RT) was seen in Figure 9d. All these findings imply its possibility of manipulating photo-stimulated

traps upon laser-free visible light stimulation in this case of tetravalent manganese doped alkali-earth metal tungstates system (see the schematic diagram in **Figure 10**).

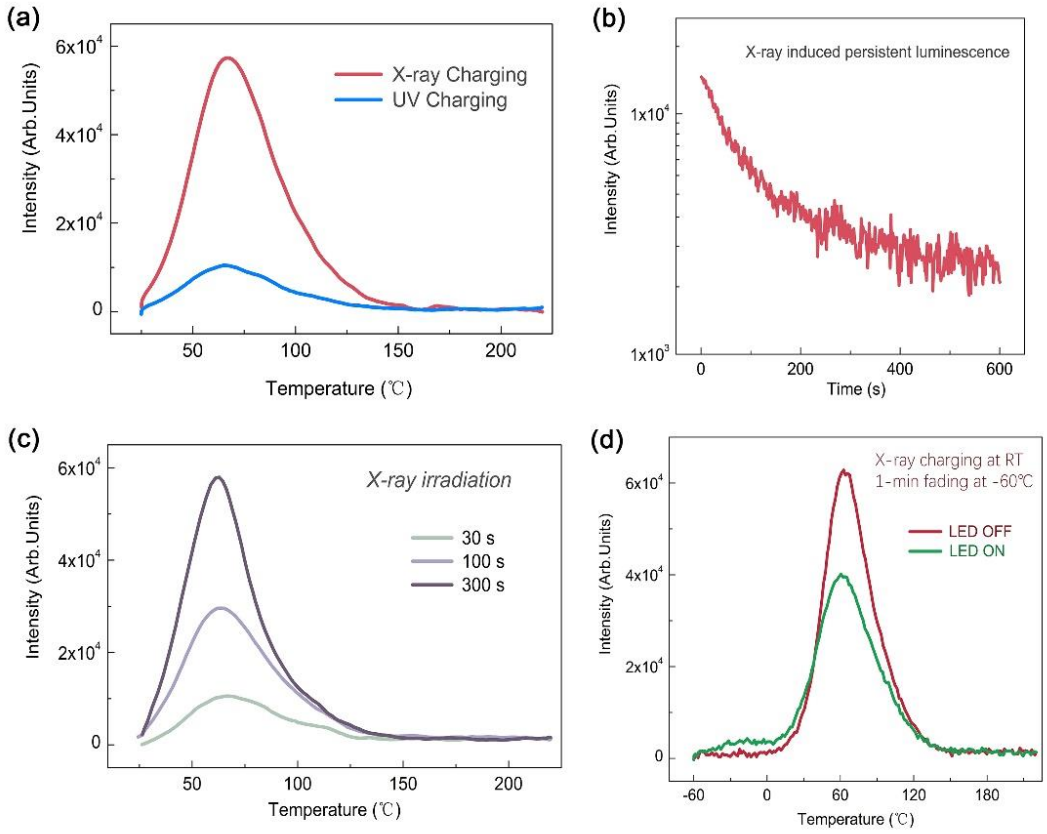

Figure 9. X-ray induced persistent luminescence and thermoluminescence of $Sr_2Ca_{0.9}La_{0.1}W_{0.995}O_6$:0.005$Mn^{4+}$. (a) TL glow curves upon X-ray or 254-nm UV irradiation, respectively; (b) persistent luminescence decay curves induced by X-ray; (c) TL glow curves upon different X-ray irradiation durations; (d) trap distribution re-shuffling by 420 nm LED stimulation.

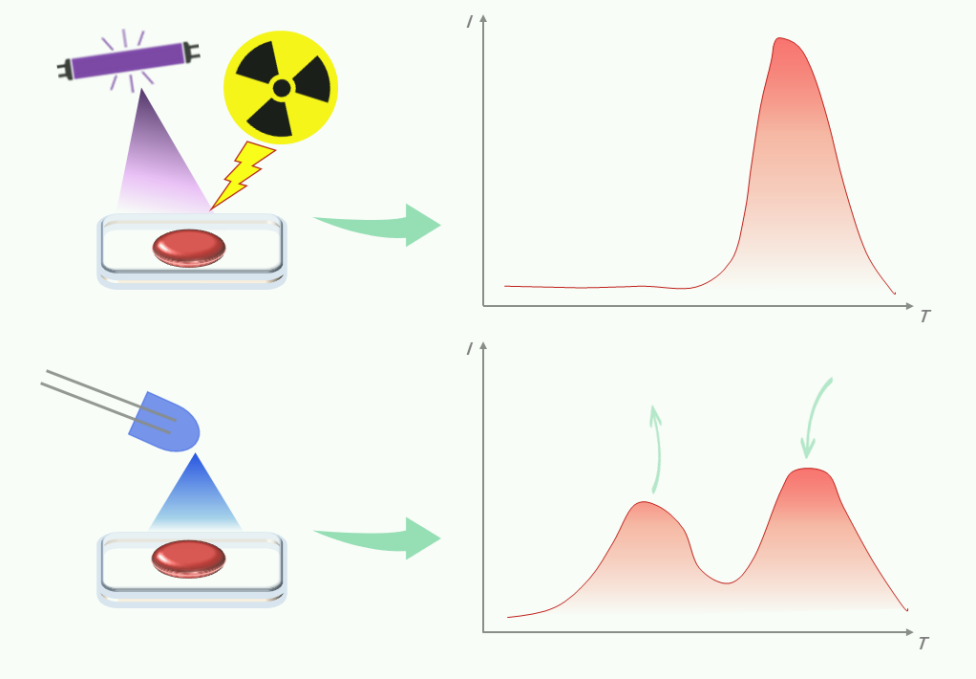

Figure 10. Schematic diagram of manipulating photo-stimulated traps via light stimulation in $Sr_2Ca_{0.9}La_{0.1}W_{0.995}O_6$:0.005$Mn^{4+}$ NIR persistent phosphor.

3. Conclusion

Near-infrared persistent luminescence was achieved in tetravalent manganese doped double-perovskite alkali-earth metal tungstates via the non-equivalent substitution of calcium ions with lanthanum ions in the lattice matrix. By employing a 420 nm light emitting diode, a photo-stimulated de-trapping process was successfully demonstrated. The trap distribution was proved to be re-shuffled upon a laser-free low intensity light stimulation. Moreover, near-infrared persistent luminescence could be generated via X-ray irradiation, providing great promise in long-term deep-tissue ultrasensitive imaging. This work is expected to offer an important guideline to design novel persistent luminescent material systems, and provides new insights into manipulation of photo-stimulated traps via laser-free light stimulation.

4. Experimental section and methods

4.1. Materials and Structural Characterizations

Phosphors with the chemical formula $Sr_2Ca_{0.9}La_{0.1}W_{0.995}O_6$:0.005$Mn^{4+}$ were prepared via high-temperature solid-state reaction according to the synthesis procedures described in our previous work[34]. Crystallographic phases of the samples were verified with powder X-ray diffraction (PXRD) measurements using a Thermo Scientific ARLX'TRA diffractometer (40 kV, 40 mA) equipped with Cu Kα1 radiation (λ= 0.154 nm). The XRD data were collected using a scanning rate of 5°/min with the scattering angle range (2θ) from 15° to 65° and the Rietveld refinement was obtained from measurements using a scanning rate of 0.6°/min in the range 2 from 5° to 90°. Details of crystal structural data and Rietveld refinements can be found in previous literature[34].

4.2. Photoluminescence, Persistent Luminescence and Thermoluminescence Characterizations

Photoluminescence excitation and emission spectra were obtained with a FS920 Edinburgh fluorescence spectrometer using a monochromated 450 W Xe-arc lamp as the excitation source. Persistent luminescence excitation spectrum was measured by monitoring at 677 nm after 3-min excitation with monochromatic light ranging from 240 to 600 nm. Persistent luminescence decay profiles were collected using a ProEM1600EMCCD camera equipped with an Acton SP2300 monochromator or a photosensor amplifier (C9329, Hamamatsu, Japan) with a Centronics OSD100-5T (Centronic Ltd., Croydon, UK) silicon photodiode. The decay intensity was calibrated into the value of the absolute radiance in unit of mW/sr/m^2 to compare among

NIR persistent phosphors. Several irradiation sources were employed for sample excitation, such as a 420 nm LED, monochromatic light at a wavelength of 365 nm, an unfiltered Xenon arc lamp or 254 nm emission line of a 3W germicidal Hg-lamp, or even X-rays from a Siemens D5000 X-ray diffractometer (Cu anode, not filtered, operated at 40 kV, 40 mA). Thermoluminescence measurements were performed in a lab-built vacuum chamber with a well-characterized cooling and heating stage. Identical size thin pellet samples (thickness ca. 2.0 mm, diameter 5.0 mm) were used and thermally conductive adhesive was added to assure good thermal contact with the heat exchanger. Prior to each experiment, a thermal cleaning of the traps was conducted by heating up to 225 °C to assure all relevant traps were empty at the start of the experiment. After each charging by excitation sources above mentioned, the sample was kept in the dark for a certain fading period with a controllable ambient temperature. A constant heating rate of 1 K s^{-1} was employed for the heating stage. A full emission spectrum with spectral shapes and intensities was recorded at each temperature by using a ProEM1600EMCCD camera connected to a 300 mm monochromator (Princeton Instruments). TL intensity was recorded by integrating the TL emission spectra from 600 nm to 800 nm. The maximum temperature of 225 °C was fixed and no higher temperature was applied to restrain the deleterious thermal quenching effects.

Supporting Information

Supporting Information is available from the author.

Acknowledgements

The authors acknowledge the financial support Ghent University's Special Research Fund (No. BOF20/PDO/015). J. Du acknowledges financial support from the Natural Science Foundation of Jiangsu Province (No. BK20210481).

References

[1] H. Bian, X. Qin, Y. Wu, Z. Yi, S. Liu, Y. Wang, C. D. S. Brites, L. D. Carlos, X. Liu, Multimodal Tuning of Synaptic Plasticity Using Persistent Luminescent Memitters. *Advanced Materials*, 2101895 (2021); doi:10.1002/adma.202101895.

[2] J. Xu, S. Tanabe, Persistent luminescence instead of phosphorescence: History, mechanism, and perspective. *Journal of Luminescence* **205**, 581-620 (2019); doi:10.1016/j.jlumin.2018.09.047.

[3] K. Van den Eeckhout, D. Poelman, P. F. Smet, Persistent luminescence in non-Eu^{2+}-doped compounds: a review. *Materials* **6**, 2789-2818 (2013); doi:10.3390/ma6072789.

[4] Y. Zhuang, L. Wang, Y. Lv, T. L. Zhou, R. J. Xie, Optical Data Storage and Multicolor Emission Readout on Flexible Films Using Deep-Trap Persistent Luminescence Materials. *Advanced Functional Materials* **28**, 1705769 (2018); doi:10.1002/adfm.201705769

[5] D. Poelman, D. V. d. Heggen, J. Du, E. Cosaert, P. F. Smet, Persistent phosphors for the future: Fit for the right application. *Journal of Applied Physics* **128**, 240903 (2020); doi:10.1063/5.0032972.

[6] L. Yuan, Y. Jin, Y. Su, H. Wu, Y. Hu, S. Yang, Optically Stimulated Luminescence Phosphors: Principles, Applications, and Prospects. *Laser & Photonics Reviews* **14**, 2000123 (2020); doi:10.1002/lpor.202000123.

[7] D. Liu, L. Yuan, Y. Jin, H. Wu, Y. Lv, G. Xiong, G. Ju, L. Chen, S. Yang, Y. Hu, Tailoring Multidimensional Traps for Rewritable Multilevel Optical Data Storage. *ACS Applied Materials & Interfaces* **11**, 35023-35029 (2019); doi:10.1021/acsami.9b13011.

[8] Y. Li, M. Gecevicius, J. Qiu, Long persistent phosphors- from fundamentals to applications. *Chemical Society Reviews* **45**, 2090-2136 (2016); doi:10.1039/C5CS00582E.

[9] J. Du, D. Poelman, Red-Light-Activated Red-Emitting Persistent Luminescence for Multicycle Bioimaging: A Case Study of CaS:Eu^{2+},Dy^{3+}. *The Journal of Physical Chemistry C* **124**, 16586-16595 (2020); doi:10.1021/acs.jpcc.0c04875.

[10] L. Huang, L. Lin, W. Xie, Z. Qiu, H. Ni, H. Liang, Q. Tang, L. Cao, J.-X. Meng, F. Li, Near-Infrared Persistent Luminescence in a Cr^{3+}-Doped Perovskite for Low-Irradiance Imaging. *Chemistry of Materials* **32**, 5579-5588 (2020); doi:10.1021/acs.chemmater.0c00807.

[11] X. Chen, Y. Li, K. Huang, L. Huang, X. Tian, H. Dong, R. Kang, Y. Hu, J. Nie, J. Qiu, G. Han, Trap Energy Upconversion-Like Near-Infrared to Near-Infrared Light Rejuvenateable Persistent Luminescence. *Advanced Materials* **33**, 2008722 (2021); doi:10.1002/adma.202008722.

[12] Y. Zhuang, Y. Lv, L. Wang, W. Chen, T. Zhou, T. Takeda, N. Hirosaki, R.-J. Xie, Trap Depth Engineering of $SrSi_2O_2N_2$:Ln^{2+},Ln^{3+} (Ln^{2+}= Yb, Eu; Ln^{3+}= Dy, Ho, Er) Persistent Luminescence Materials for Information Storage Applications. *ACS Applied Materials & Interfaces* **10**, 1854-1864 (2018); doi:10.1021/acsami.7b17271.

[13] T. Shi, W. Sun, R. Qin, D. Li, Y. Feng, L. Chen, G. Liu, X. Chen, H. Chen, X-Ray-Induced Persistent Luminescence Promotes Ultrasensitive Imaging and Effective Inhibition of Orthotopic Hepatic Tumors. *Advanced Functional Materials* **30**, 2001166 (2020); doi:10.1002/adfm.202001166.

[14] H. Chen, X. Sun, G. D. Wang, K. Nagata, Z. Hao, A. Wang, Z. Li, J. Xie, B. Shen, $LiGa_5O_8$:Cr-based theranostic nanoparticles for imaging-guided X-ray induced photodynamic therapy of deep-seated tumors. *Materials Horizons* **4**, 1092-1101 (2017); doi:10.1039/c7mh00442g.

[15] B.-M. Liu, R. Zou, S.-Q. Lou, Y.-F. Gao, L. Ma, K.-L. Wong, J. Wang, Low-dose X-ray-stimulated $LaGaO_3$:Sb,Cr near-infrared persistent luminescence nanoparticles for deep-tissue and renewable in vivo bioimaging. *Chemical Engineering Journal* **404**, 127133 (2021); doi:10.1016/j.cej.2020.127133.

[16] P. Pei, Y. Chen, C. Sun, Y. Fan, Y. Yang, X. Liu, L. Lu, M. Zhao, H. Zhang, D. Zhao, X. Liu, F. Zhang, X-ray-activated persistent luminescence nanomaterials for NIR-II imaging. *Nature Nanotechnology*, (2021); doi:10.1038/s41565-021-00922-3.

[17] S. Ding, H. Guo, P. Feng, Q. Ye, Y. Wang, A New Near-Infrared Long Persistent Luminescence Material with Its Outstanding Persistent Luminescence Performance and Promising Multifunctional Application Prospects. *Advanced Optical Materials* **8**, 2000097 (2020); doi:10.1002/adom.202000097.

[18] J. Meyer, F. Tappe, Photoluminescent Materials for Solid-State Lighting: State of the Art and Future Challenges. *Advanced Optical Materials* **3**, 424-430 (2015); doi:10.1002/adom.201400511.

[19] S. Adachi, Mn^{4+} and Cr^{3+} ions in red and deep red-emitting phosphors: Spectral analysis and Racah parameter determination. *Journal of Luminescence* **223**, 117217 (2020); doi:10.1016/j.jlumin.2020.117217.

[20] Z. Zhou, Y. Li, M. Peng, Near-infrared persistent phosphors: Synthesis, design, and applications. *Chemical Engineering Journal* **399**, 125688 (2020); doi:doi.org/10.1016/j.cej.2020.125688.

[21] Y. Zhuang, Y. Katayama, J. Ueda, S. Tanabe, A brief review on red to near-infrared persistent luminescence in transition-metal-activated phosphors. *Optical Materials* **36**, 1907-1912 (2014); doi:10.1016/j.optmat.2014.05.035.

[22] T. Maldiney, B. T. Doan, D. Alloyeau, M. Bessodes, D. Scherman, C. Richard, Gadolinium‐Doped Persistent Nanophosphors as Versatile Tool for Multimodal In Vivo Imaging. *Advanced Functional Materials* **25**, 331-338 (2015); doi:10.1002/adfm.201401612.

[23] Z. Pan, Y.-Y. Lu, F. Liu, Sunlight-activated long-persistent luminescence in the near-infrared from Cr^{3+}-doped zinc gallogermanates. *Nature Materials* **11**, 58 (2012); doi:10.1038/nmat3173.

[24] H. Lin, G. Bai, T. Yu, M.-K. Tsang, Q. Zhang, J. Hao, Site Occupancy and Near-Infrared Luminescence in $Ca_3Ga_2Ge_3O_{12}$:Cr^{3+} Persistent Phosphor. *Advanced Optical Materials* **5**, 1700227 (2017); doi:10.1002/adom.201700227.

[25] T. Maldiney, A. Bessière, J. Seguin, E. Teston, S. K. Sharma, B. Viana, A. J. Bos, P. Dorenbos, M. Bessodes, D. Gourier, D. Scherman, C. Richard, The in vivo activation of persistent nanophosphors for optical imaging of vascularization, tumours and grafted cells. *Nature Materials* **13**, 418 (2014); doi:10.1038/nmat3908.

[26] Y. Zhao, J. Du, X. Wu, Y. Wang, D. Poelman, Enhanced near-infrared persistent luminescence in $MgGa_2O_4$:Cr^{3+} through codoping. *Journal of Luminescence* **220**, 117035 (2020); doi:10.1016/j.jlumin.2020.117035.

[27] F. Liu, W. Yan, Y.-J. Chuang, Z. Zhen, J. Xie, Z. Pan, Photostimulated near-infrared persistent luminescence as a new optical read-out from Cr^{3+}-doped $LiGa_5O_8$. *Scientific Reports* **3**, 1554 (2013); doi:10.1038/srep01554.

[28] M. Allix, S. b. Chenu, E. Véron, T. Poumeyrol, E. A. Kouadri-Boudjelthia, S. Alahrache, F. Porcher, D. Massiot, F. Fayon, Considerable improvement of long-persistent luminescence in germanium and tin substituted $ZnGa_2O_4$. *Chemistry of Materials* **25**, 1600-1606 (2013); doi:10.1021/cm304101n.

[29] J. Du, D. Poelman, Identifying Near-Infrared Persistent Luminescence in Cr^{3+}-Doped Magnesium Gallogermanates Featuring Afterglow Emission at Extremely Low Temperature. *Advanced Optical Materials* **8**, 1901848 (2020); doi:10.1002/adom.201901848.

[30] Y. Katayama, B. Viana, D. Gourier, J. Xu, S. Tanabe, Photostimulation induced persistent luminescence in $Y_3Al_2Ga_3O_{12}:Cr^{3+}$. *Optical Materials Express* **6**, 1405-1413 (2016); doi:10.1364/OME.6.001405.

[31] L. Liang, N. Chen, Y. Jia, Q. Ma, J. Wang, Q. Yuan, W. Tan, Recent progress in engineering near-infrared persistent luminescence nanoprobes for time-resolved biosensing/bioimaging. *Nano Research* **12**, 1279-1292 (2019); doi:10.1007/s12274-019-2343-6.

[32] J. Du, D. Poelman, Facile Synthesis of Mn^{4+}-Activated Double Perovskite Germanate Phosphors with Near-Infrared Persistent Luminescence. *Nanomaterials* **9**, 1759 (2019); doi:10.3390/nano9121759.

[33] Y. Li, Y.-Y. Li, K. Sharafudeen, G.-P. Dong, S.-F. Zhou, Z.-J. Ma, M.-Y. Peng, J.-R. Qiu, A strategy for developing near infrared long-persistent phosphors: taking $MAlO_3$: Mn^{4+}, Ge^{4+} (M= La, Gd) as an example. *Journal of Materials Chemistry C* **2**, 2019-2027 (2014); doi: 10.1039/C3TC32075H.

[34] K. Li, J. Du, D. Poelman, H. Vrielinck, D. Mara, R. Van Deun, Achieving Efficient Red-Emitting $Sr_2Ca_{1-\delta}Ln_\delta WO_6:Mn^{4+}$ (Ln = La, Gd, Y, Lu, δ = 0.10) Phosphors with Extraordinary Luminescence Thermal Stability for Potential UV-LEDs Application via Facile Ion Substitution in Luminescence-Ignorable $Sr_2CaWO_6:Mn^{4+}$. *ACS Materials Letters* **2**, 771-778 (2020); doi:10.1021/acsmaterialslett.0c00212.

[35] S. Adachi, Mn^{4+}-Activated Red and Deep Red-Emitting Phosphors. *ECS Journal of Solid State Science and Technology* **9**, 016001 (2020); doi:10.1149/2.0022001JSS.

[36] S. Adachi, Photoluminescence properties of Mn^{4+}-activated oxide phosphors for use in white-LED applications: A review. *Journal of Luminescence* **202**, 263-281 (2018); doi:10.1016/j.jlumin.2018.05.053.

[37] Y. Tanabe, S. Sugano, On the Absorption Spectra of Complex Ions. I. *Journal of the Physical Society of Japan* **9**, 753-766 (1954); doi:10.1143/JPSJ.9.753.

[38] Y. Tanabe, S. Sugano, On the absorption spectra of complex ions II. *Journal of the Physical Society of Japan* **9**, 766-779 (1954); doi:10.1143/JPSJ.9.766.

[39] J. Du, O. Q. De Clercq, D. Poelman, Temperature dependent persistent luminescence: Evaluating the optimum working temperature. *Scientific Reports* **9**, 10517 (2019); doi:10.1038/s41598-019-46889-z.

[40] J. Du, O. Q. De Clercq, K. Korthout, D. Poelman, $LaAlO_3:Mn^{4+}$ as Near-Infrared Emitting Persistent Luminescence Phosphor for Medical Imaging: A Charge Compensation Study. *Materials* **10**, 1422 (2017); doi:10.3390/ma10121422.

[41] J. Du, D. Poelman, Near-infrared persistent luminescence in Mn^{4+} doped perovskite type solid solutions. *Ceramics International* **45**, 8345-8353 (2019); doi:10.1016/j.ceramint.2019.01.142.

[42] K. Van den Eeckhout, A. J. Bos, D. Poelman, P. F. Smet, Revealing trap depth distributions in persistent phosphors. *Physical Review B* **87**, 045126 (2013); doi:10.1103/PhysRevB.87.045126.

[43] J. Botterman, J. J. Joos, P. F. Smet, Trapping and detrapping in $SrAl_2O_4$:Eu,Dy persistent phosphors: Influence of excitation wavelength and temperature. *Physical Review B* **90**, 085147 (2014); doi:doi.org/10.1103/PhysRevB.90.085147.

[44] J. Du, A. Feng, D. Poelman, Temperature Dependency of Trap-Controlled Persistent Luminescence. *Laser & Photonics Reviews* **14**, 2000060 (2020); doi:10.1002/lpor.202000060.

[45] R. R. Petit, S. E. Michels, A. Feng, P. F. Smet, Adding memory to pressure-sensitive phosphors. *Light: Science & Applications* **8**, 124 (2019); doi:10.1038/s41377-019-0235-x.

[46] Y. Zhuang, D. Tu, C. Chen, L. Wang, H. Zhang, H. Xue, C. Yuan, G. Chen, C. Pan, L. Dai, R.-J. Xie, Force-induced charge carrier storage: a new route for stress recording. *Light: Science & Applications* **9**, 182 (2020); doi:10.1038/s41377-020-00422-4.

[47] J. Xu, D. Murata, J. Ueda, B. Viana, S. Tanabe, Toward Rechargeable Persistent Luminescence for the First and Third Biological Windows via Persistent Energy Transfer and Electron Trap Redistribution. *Inorganic Chemistry* **57**, 5194-5203 (2018); doi:10.1021/acs.inorgchem.8b00218.

The table of contents entry

Manipulating trap distribution upon visible light stimulation is achieved in persistent luminescent Mn^{4+} doped double-perovskite alkali-earth metal tungstates. Photo-stimulated de-trapping is demonstrated by a common 420 nm LED and the traps distribution is re-shuffled. This work is expected to broaden the range of near-infrared persistent material systems and provides new insights into manipulating photo-stimulated traps via laser-free visible light stimulation.

Jiaren Du*, Kai Li, Rik Van Deun, Dirk Poelman*, Hengwei Lin

Near-infrared Persistent Luminescence and Trap Re-shuffling in Mn^{4+} Doped Alkali-earth Metal Tungstates

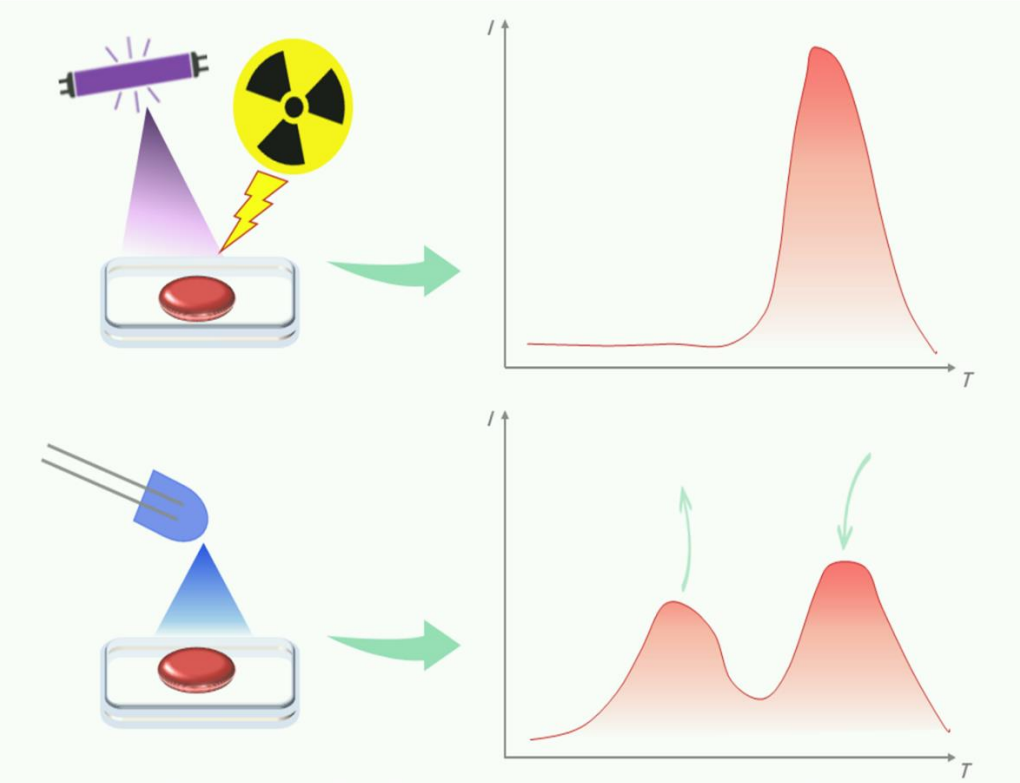

Manipulating Trap Distribution upon Visible Light Stimulation